Explaining inter-annual variability of gross primary productivity from plant phenology and physiology

Sha Zhou [a,b,*], Yao Zhang [c], Kelly K. Caylor [b], Yiqi Luo [d,e], Xiangming Xiao [c,f], Philippe Ciais [g], Yuefei Huang [a,h,*], Guangqian Wang [a]

[a] State Key Laboratory of Hydroscience and Engineering, Department of Hydraulic Engineering, Tsinghua University, Beijing 100084, China
[b] Department of Civil and Environmental Engineering, Princeton University, Princeton, NJ 08544, USA
[c] Department of Microbiology and Plant Biology, Center for Spatial Analysis, University of Oklahoma, Norman, OK 73019, USA
[d] Department of Microbiology and Plant Biology, University of Oklahoma, Norman, OK 73019, USA
[e] Center for Earth System Science, Tsinghua University, Beijing 100084, China
[f] Instittue of Biodiversity Science, Fudan University, Shanghai 200433, China
[g] Laboratoire des Sciences du Climat et de l'Environnement, CEA CNRS UVSQ, Gif-sur-Yvette 91190, France
[h] College of Ecological and Environmental Engineering, Qinghai University, Xining 810086 Qinghai, China

ARTICLE INFO

ABSTRACT

Climate variability influences both plant phenology and physiology, resulting in inter-annual variation in terrestrial gross primary productivity (GPP). However, it is still difficult to explain the inter-annual variability of GPP. In this study, we propose a Statistical Model of Integrated Phenology and Physiology (SMIPP) to explain the contributions of maximum daily GPP (GPP_{max}), and start and end of the growing season (GS_{start} and GS_{end}) to the inter-annual variability of GPP observed at 27 sites across North America and Europe. Strong relationships are found between the anomalies of GS_{start} and spring GPP ($r = 0.82 \pm 0.10$), GPP_{max} and summer GPP ($r = 0.90 \pm 0.14$), and GS_{end} and autumn GPP ($r = 0.75 \pm 0.18$) within each site. Partial correlation analysis further supports strong correlations of annual GPP with GS_{start} (partial r value being 0.72 ± 0.20), GPP_{max} (0.87 ± 0.15), and GS_{end} (0.59 ± 0.26), respectively. In addition, the three indicators are found independent from each other to influence annual GPP at most of the 27 sites. Overall, the site-calibrated SMIPP explains $90 \pm 11\%$ of the annual GPP variability among the 27 sites. In general, GPP_{max} contributes to annual GPP variation more than the two phenological indicators. These results indicate that the inter-annual variability of GPP can be effectively estimated using the three indicators. Investigating plant physiology, and spring and autumn phenology to environmental changes can improve the prediction of the annual GPP trajectory under future climate change.

© 2016 Elsevier B.V. All rights reserved.

1. Introduction

Global carbon cycle exhibits strong inter-annual variability, most of which has been inferred to be caused by changes in carbon sequestration in terrestrial ecosystems (Ballantyne et al., 2012). Indeed, the inter-annual variability is one of the least understood carbon cycle processes (Luo et al., 2015). Past researches have been focused on the timings of spring emergence and autumn senescence under global warming, which were found to shift in the Northern Hemisphere, and the length of growing season has changed (Cleland et al., 2007; Ibáñez et al., 2010). Growing season length has substantial effects on annual carbon uptake; both gross primary productivity (GPP) and net ecosystem productivity (NEP) are enhanced by longer growing seasons caused by warming climate (Churkina et al., 2005; Dragoni et al., 2011; Keenan et al., 2014; Piao et al., 2007; Richardson et al., 2010). In addition, warming-induced drought stress limits plant photosynthesis in summer and leads to great decline in peak summer productivity and even annual GPP (Angert et al., 2005; Buermann et al., 2013; Ciais et al., 2005; Schwalm et al., 2012). Since both phenology dates and photosynthetic physiology greatly affect annual GPP, it is necessary to explain annual GPP variability from both plant phenology and physiology yet to partition their respective contributions.

Recently, Xia et al. (2015) proposed that annual GPP is jointly controlled by plant phenology and physiology and can be diag-

* Corresponding authors at: State Key Laboratory of Hydroscience and Engineering, Department of Hydraulic Engineering, Tsinghua University, Beijing 100084, China
  E-mail addresses: zhous13@mails.tsinghua.edu.cn (S. Zhou),
yuefeihuang@tsinghua.edu.cn (Y. Huang).

nosed by the product of the length of CO_2 uptake period (CUP) and the maximum capacity of CO_2 uptake (GPP_{max}). The product of CUP and GPP_{max}, i.e., $CUP \times GPP_{max}$, can explain more than 90% of the temporal GPP variability in most areas of North America during 2000–2010 and more than 95% of the spatial GPP variation among 213 flux tower sites. Although CUP is a good phenological indicator, it does not allow us to separately evaluate the influence of spring and autumn phenology on annual GPP variability. While CUP does not change, spring emergence and autumn senescence may shift and affect annual GPP in different ways (Richardson et al., 2010). In addition, the respective contributions of spring emergence and autumn senescence to growing season change and hence annual GPP variability have not been separated, and their contributions seem to vary across different ecosystems (Garonna et al., 2014; Jeong et al., 2011; Menzel and Fabian, 1999; Zhu et al., 2012). Thus, the effects of both spring emergence and autumn senescence on annual GPP should be considered separately to investigate the contributions of spring and autumn phenological changes to the inter-annual variability of GPP.

In northern temperate ecosystems, the growing season starts in spring and ends in autumn when the photosynthetic carbon assimilation is limited by temperature and solar radiation. Daily photosynthetic rate reaches its peak (GPP_{max}) in summer under favorable environmental conditions, and GPP is small or even negligible in winter (Allard et al., 2008; Hirata et al., 2007; Saigusa et al., 2008; Uehlinger, 2006). The starting and ending dates of the growing season, expressed by GS_{start} and GS_{end}, are closely correlated with spring and autumn GPP, respectively (Keenan et al., 2014). Similarly, GPP_{max} is positively correlated with summer GPP (Stoy et al., 2014). Thus, the three indicators, GS_{start}, GPP_{max}, and GS_{end}, can influence seasonal GPP and hence annual GPP. Combining the effects of these three indicators, it may have the potential to explain annual GPP variability and separate the respective contributions of both spring and autumn phenology and plant physiology to it.

Because the phenological and physiological events occur in different seasons and affect carbon assimilation in different ways, these three indicators may have independent effects on annual GPP. The spring emergence and autumn senescence dates vary temporally and spatially, and respond differently to climate change (Vitasse et al., 2009). Although there is a strong correlation between warmer temperature and earlier spring emergence, the association between temperature and autumn senescence is weaker (Menzel et al., 2006). In addition to temperature, spring emergence is also affected by other factors, such as winter chilling conditions and freeze-thaw processes (Chen et al., 2011; Fu et al., 2015; Pope et al., 2013; Yi and Zhou, 2011; Yu et al., 2010). Autumn senescence has been reported to be influenced by multiple factors, including temperature, precipitation, photoperiod, soil moisture, wind, frost events, etc. (Fracheboud et al., 2009; Panchen et al., 2015; Yang et al., 2015). In view of the different responses to climate factors, both spring emergence and autumn senescence should be included and the combination of the three indicators could provide more exhaustive explanation of annual GPP variability.

This paper proposes an integrated statistical model to explain the inter-annual variability of GPP in the Northern Hemisphere from the perspectives of both phenology and physiology and evaluates the contributions of phenological and physiological changes to annual GPP variability using data from 27 flux tower sites (283 site-years) across North America and Europe. The specific objectives are to (1) investigate the effects of variations in GS_{start}, GPP_{max} and GS_{end} on respective seasonal GPP and hence annual GPP; (2) develop a Statistical Model of Integrated Phenology and Physiology (SMIPP) involving the three indicators to explain the inter-annual variability of GPP for each site; (3) partition the contributions of

phenological and physiological changes to annual GPP variability for the 283 site-years.

2. Materials and methods

2.1. Flux tower data

GPP estimates ($g\,C\,m^{-2}\,day^{-1}$) were obtained from 14 AmeriFlux sites and 13 EuroFlux sites (Table 1). A total of 283 site-years were used and the record length for each site ranged from 6 to 21 years. Generally, the 27 flux sites were classified into three plant functional types, including 8 deciduous broadleaf forests (DBF), 9 evergreen needle-leaf forests (ENF), and 10 non-forests sites (NF) (e.g., cropland, grassland, closed shrubland and wetland). The estimates of GPP were available from AmeriFlux (Level 2 products, http://public.ornl.gov/ameriflux) and EuroFlux (Level 4 products, http://gaia.agraria.unitus.it/). The half-hourly eddy covariance measurements (i.e., net ecosystem exchange) used in this study have been standardized, gap-filled using the Marginal Distribution Sampling (MDS) method, and partitioned into GPP and ecosystem respiration (Papale and Valentini, 2003; Reichstein et al., 2005).

The 27 sites were chosen according to the following four criteria. (1) The site-years with more than 80% of the GPP data which were actual measurements or gap-filled with high confidence, i.e., data marked as 'the original' or 'most reliable' according to the quality flag, were selected. Only the site-years with effective measurements covering the entire growing season (March-October) were used. (2) The sites with at least 6 site-years of data were selected in order to avoid overfitting of multiple linear regression. According to Austin and Steyerberg (2015), a minimum of two observations per variable is required to permit accurate estimation of regression coefficients (relative bias < 10%). As three variables (GS_{start}, GPP_{max} and GS_{end}) were used to build up the regression, 6 years of observations for each site is the minimum requirement. (3) Sites located in the moist tropical climate with low seasonality of daily GPP were not used because the phenology dates cannot be identified according to the given threshold. (4) Sites located in some Mediterranean climate were not used because the maximum daily GPP occurs during the winter-spring seasons.

The half-hourly data of GPP were aggregated to daily totals. The following subsequent steps were taken: (1) seasonal and annual GPP were calculated for each site-year; for seasonal analysis, spring refers to March-May, summer refers to June-August, autumn refers to September-November, and the remaining months are considered as winter; (2) the time series of daily GPP over each site-year were smoothed using singular spectrum analysis (SSA) to identify the three indicators GS_{start}, GPP_{max} and GS_{end}; (3) Pearson correlation was used to develop the relationship between the anomalies of the three indicators and their respective seasonal GPP; Pearson partial correlation was used to develop the relationship between the anomalies of annual GPP and each of the three indicators; (4) the interrelationship between each pair of the three indicators was investigated to test whether the three indicators are independent from each other; (5) a multiple regression model was established between the anomalies of annual GPP and the three indicators to explain the inter-annual variability of GPP and separate the contributions of the three indicators for each site.

2.2. Statistical model of integrated phenology and physiology

The Statistical Model of Integrated Phenology and Physiology (SMIPP) to explain the inter-annual variability of GPP is an extension of the approach of Xia et al. (2015), i.e., $GPP = \alpha \cdot CUP \cdot GPP_{max}$.

Table 1

Twenty-seven eddy covariance sites in North America and Europe used in this study. Site descriptions include Site Identifier (ID), Latitude (Lat, °), Longitude (Lon, °), Plant Functional Type (PFT), Period of Record, and a reference for each site. PFTs are taken from the International Geosphere-Biosphere Program (IGBP) land cover classification scheme (DBF = Deciduous Broadleaf Forest, ENF = Evergreen Needle-Leaf Forest, CRO = Cropland, GRA = Grassland, CSH = Closed Shrub Land, WET = Wetland).

Site ID	Lat	Lon	PFT	Period of Record	Reference
DE-Hai	51.0792	10.4530	DBF	2000–2007	Kutsch et al. (2008)
IT-Col	41.8494	13.5881	DBF	1998/2000–2002/2005/2007–2012	Valentini et al. (1996)
IT-Ro2	42.3903	11.9209	DBF	2002–2008/2010–2012	Gioli et al. (2004)
US-Ha1	42.5378	−72.1715	DBF	1992–2012	Urbanski et al. (2007)
US-MMS	39.3231	−86.4131	DBF	1999–2014	Dragoni et al. (2007)
US-PFa	45.9459	−90.2723	DBF	1997–2004/2006–2014	Saito et al. (2009)
US-UMd	45.5625	−84.6975	DBF	2007–2013	Nave et al. (2011)
US-WCr	45.8060	−90.0798	DBF	1999–2006/2011–2014	Yi et al. (2004)
BE-Bra	51.3092	4.5206	ENF	1999–2000/2002/2004–2008	Carrara et al. (2004)
CA-Qcu	49.2671	−74.0365	ENF	2002–2009	Giasson et al. (2006)
CA-Qfo	49.6925	−74.3420	ENF	2004–2009	Bergeron et al. (2007)
CH-Dav	46.8153	9.8559	ENF	1998–2009	Zweifel et al. (2010)
FI-Sod	67.3619	26.6378	ENF	2000–2008	Thum et al. (2007)
IT-Ren	46.5869	11.4337	ENF	1999/2001–2011	van Gorsel et al. (2009)
RU-Fyo	56.4615	32.9221	ENF	1999–2010	Groenendijk et al. (2009)
US-Ho1	45.2041	−68.7402	ENF	1996–2004/2006–2008	Hollinger et al. (2004)
US-Ho2	45.2091	−68.7470	ENF	1999–2009	Richardson and Hollinger (2005)
US-Ne1	41.1650	−96.4766	CRO	2002–2012	Suyker et al. (2005)
US-Ne2	41.1649	−96.4701	CRO	2001–2012	Suyker et al. (2005)
US-Ne3	41.1797	−96.4396	CRO	2001–2012	Suyker et al. (2005)
AT-Neu	47.1167	11.3175	GRA	2002–2009	Wohlfahrt et al. (2008)
IT-MBo	46.0147	11.0458	GRA	2003–2012	Gilmanov et al. (2007)
SE-Deg	64.1820	19.5567	GRA	2001–2003/2005–2009	Lund et al. (2010)
UK-AMo	55.7917	−3.2389	GRA	2003/2005–2010	Stoy et al. (2013)
US-Kon	39.0824	−96.5603	GRA	2007–2012	Scurlock et al. (2002)
US-Los	46.0827	−89.9792	CSH	2001–2008	Liang et al. (2006)
FI-Kaa	69.1407	27.2950	WET	2000–2008	Aurela et al. (2004)

Firstly, annual GPP is expressed as a function of GS_{start}, GPP_{max}, and GS_{end}

$$GPP = f(GS_{start}, GPP_{max}, GS_{end}) \qquad (1)$$

The three indicators GS_{start}, GPP_{max} and GS_{end} are assumed to be independent from each other and that their combination includes the phenological and physiological changes of plants under environmental changes. The total differential form of annual GPP with respect to the three indicators is as follows:

$$dGPP = \frac{\partial GPP}{\partial GS_{start}} dGS_{start} + \frac{\partial GPP}{\partial GPP_{max}} dGPP_{max} + \frac{\partial GPP}{\partial GS_{end}} dGS_{end} \qquad (2)$$

Transforming the absolute changes in annual GPP and the three indicators into their relative forms, the relative change in annual GPP can be evaluated as

$$\frac{dGPP}{\overline{GPP}} = \frac{\partial GPP/\overline{GPP}}{\partial GS_{start}/\overline{GS_{start}}} \frac{dGS_{start}}{\overline{GS_{start}}} + \frac{\partial GPP/\overline{GPP}}{\partial GPP_{max}/\overline{GPP_{max}}} \frac{dGPP_{max}}{\overline{GPP_{max}}}$$
$$+ \frac{\partial GPP/\overline{GPP}}{\partial GS_{end}/\overline{GS_{end}}} \frac{dGS_{end}}{\overline{GS_{end}}}$$

or

$$\frac{dGPP}{\overline{GPP}} = m_{start} \frac{dGS_{start}}{\overline{GS_{start}}} + m_{gpp} \frac{dGPP_{max}}{\overline{GPP_{max}}} + m_{end} \frac{dGS_{end}}{\overline{GS_{end}}} \qquad (3)$$

where $\overline{GS_{start}}$, $\overline{GPP_{max}}$, $\overline{GS_{end}}$ and $\overline{GPP}$ refer to the mean annual values of the three indicators and annual GPP, and are constant for a given site. The parameters m_{start} ($\frac{\partial GPP/\overline{GPP}}{\partial GS_{start}/\overline{GS_{start}}}$), m_{gpp} ($\frac{\partial GPP/\overline{GPP}}{\partial GPP_{max}/\overline{GPP_{max}}}$) and m_{end} ($\frac{\partial GPP/\overline{GPP}}{\partial GS_{end}/\overline{GS_{end}}}$) are the sensitivity coefficients of annual GPP relative to $\overline{GS_{start}}$, $\overline{GPP_{max}}$ and $\overline{GS_{end}}$, respectively, representing the conversion factors from the relative changes in the three indicators to the relative change in annual GPP. Eq. (3) indicates that the inter-annual variability of GPP can be decomposed into three independent components, induced by the changes in the three indicators. The phenological and physiological sensitivity coefficients
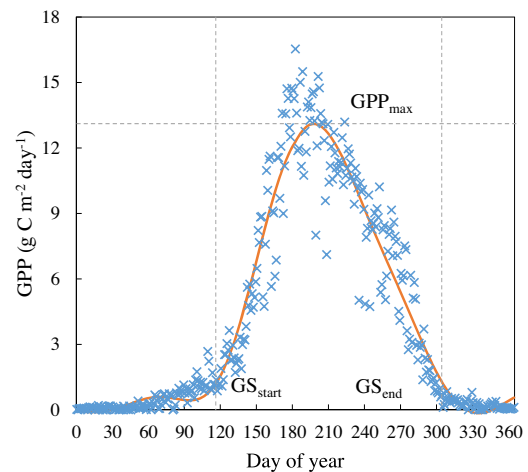

Fig. 1. An example of the reconstructed time series of daily gross primary productivity (GPP) using the singular spectrum analysis method, and determination of the three phenological and physiological indicators, i.e., GS_{start}, GPP_{max} and GS_{end} at the US-Ha1 (DBF) site in 2002.

of annual GPP in the SMIPP were estimated using the multiple regression method, where $dGPP/\overline{GPP}$ is the dependent variable and $dGS_{start}/\overline{GS_{start}}$, $dGPP_{max}/\overline{GPP_{max}}$, $dGS_{end}/\overline{GS_{end}}$ are the independent variables.

2.3. Determination of phenological and physiological indicators

Values for GS_{start}, GS_{end} and GPP_{max} were determined from time series of GPP for each site-year. Singular spectrum analysis (SSA) was used to derive smoothed curves from daily GPP measurements (Fig. 1). The SSA is a non-parametric method for the analysis of time series. It can decompose a time series into oscillatory components and noises according to the singular value decomposition, and then reconstruct specific components (e.g., seasonal signal) from the original time series (Vautard et al., 1992). The SSA method

has been used to identify the phenological transition dates from time series of GPP in previous studies (Keenan et al., 2014). The "Rssa" package in R (https://cran.r-project.org/web/packages/Rssa/index.html) provides a set of fast and reliable tools to perform SSA, and it was used to decompose and reconstruct the time series of GPP and obtain a smoothed curve of daily GPP for each site-year.

GPP_{max} was determined as the peak value of the smoothed curve of daily GPP. GS_{start} and GS_{end} were determined as the first and last days when the smoothed daily GPP crossed a given threshold. In this study, the threshold was set to be 10% of the multi-year average GPP_{max} over all available years for each site, and it varied from 0.5 to 2.5 g C m^{-2} day^{-1} among different sites. The choice of this threshold was determined by comparing with other approaches. In comparison with fixed thresholds across all sites (e.g., 2 g C m^{-2} day^{-1} in Richardson et al. (2010)), relative thresholds for individual sites can better capture variations in phenological events without being affected by different vegetation types and sites, because GPP_{max} varies considerably (5–25 g C m^{-2} day^{-1}) among different sites. Keenan et al. (2014) used 30% of mean annual variance of daily GPP as a threshold for each site, and stated that the inter-annual variability of the derived phenological dates is not affected by the threshold value, which only impacts the mean estimated dates for each site. Compared with a variable threshold, such as 10% of GPP_{max} for each year in Wu et al. (2013), a fixed threshold, i.e., 10% of the multi-year average GPP_{max}, for each site used in this study can better reflect the inter-annual variability in phenological transition dates and avoid artificially induced interrelationship among the three indicators.

2.4. Absolute and relative anomaly analyses

An anomaly analysis was performed to represent the inter-annual variability of GPP and other variables. Both the absolute and relative anomalies were used in this study. The absolute anomaly refers to the deviation of a variable from its mean value, while the relative anomaly is the standardized deviation of a variable from its mean value. The two kinds of anomalies are calculated as follows:

$$\Delta X_i = X_i - \bar{X} \qquad (4)$$

$$\delta X_i = \frac{X_i - \bar{X}}{\bar{X}} \times 100\% \qquad (5)$$

where X_i represents the variable X in year i, and $\bar{X}$ is the mean annual value of the variable X over all the available years for each site. ΔX_i and δX_i represent the absolute and relative anomalies of X_i, respectively. The absolute anomalies of seasonal and annual GPP, and the three indicators GS_{start}, GPP_{max} and GS_{end}, were calculated for correlation analysis. Relative anomalies of the three independent variables and one dependent variable in Eq. (3) were used to establish the SMIPP for each of the 27 sites.

To make the absolute and relative anomalies of GS_{start} and GS_{end} more comparable, they were calculated in the following ways:

$$\Delta GS_{start} = \overline{GS_{start}} - GS_{start} \qquad (6)$$

$$\Delta GS_{end} = GS_{end} - \overline{GS_{end}} \qquad (7)$$

$$\delta GS_{start} = \frac{\Delta GS_{start}}{\overline{GS_{start}}} \times 100\% \qquad (8)$$

$$\delta GS_{end} = \frac{\Delta GS_{end}}{365 - \overline{GS_{end}}} \times 100\% \qquad (9)$$

The absolute anomalies in Eqs. (6) and (7) would be positive when GS_{start} advances and GS_{end} delays relative to their mean values, which both contribute positively to annual GPP increase. The relative anomalies of GS_{start} and GS_{end} in Eqs. (8) and (9) were used as the independent variables of the SMIPP in Eq. (3).
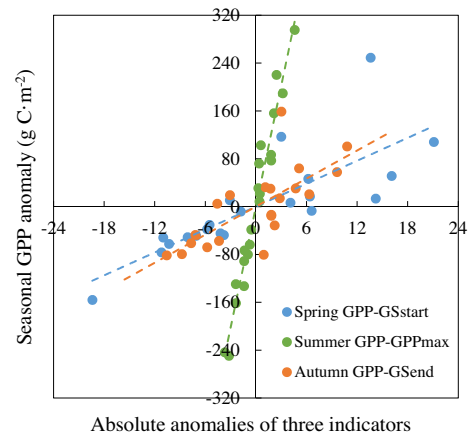

Fig. 2. An example of the linear relationship between the absolute anomalies of GS_{start} (day) and spring GPP, GPP_{max} (g C m^{-2} day^{-1}) and summer GPP, GS_{end} (day) and autumn GPP, respectively, at the US-Ha1 site.

3. Results

3.1. Relationship between the anomalies of GPP and the three indicators

The absolute anomalies of the two phenological indicators, GS_{start} and GS_{end}, and of the physiological indicator, GPP_{max}, were used to explain inter-annual variations in seasonal GPP and hence annual GPP. For example, Fig. 2 shows the relationship between absolute anomalies of the three indicators and corresponding seasonal GPP at the US-Ha1 site. Similarly, the three indicators were used to explain the GPP variability across the three PFTs and the 27 sites.

The correlation results between the anomalies of the three indicators and their respective seasonal GPP for the 27 sites are shown in Fig. 3. GPP_{max} shows a strong correlation with summer GPP (0.90 ± 0.14), and the correlation coefficient is more than 0.80 for 24 out of the 27 sites, except for two DBF sites (DE-Hai and IT-Ro2) and one NF site (US-Ne1). The two phenological indicators do not explain spring and autumn GPP variations so well as GPP_{max} explains summer GPP variation. And GS_{start} correlates with spring GPP (r = 0.82 ± 0.10) more closely than GS_{end} with autumn GPP (r = 0.75 ± 0.18). The linear relationship between GPP_{max} and summer GPP is stronger for ENF (r = 0.95 ± 0.03) sites than for DBF (r = 0.83 ± 0.20) and NF (r = 0.90 ± 0.11) sites. Although GPP_{max} explains summer GPP well for ENF sites, the two phenological indicators explain spring and autumn GPP less well for ENF than for the other two PFTs (Fig. 3a–c). NF sites show the highest correlation coefficients between GS_{start} and spring GPP (0.86 ± 0.08) and between GS_{end} and autumn GPP (0.83 ± 0.11).

The increase in GPP_{max} leads to more carbon assimilation in summer for ENF sites, where 1 g C m^{-2} day^{-1} increase in GPP_{max} corresponds to an increase of 79.3 ± 9.2 g C m^{-2} in summer GPP. The sensitivity of summer GPP to GPP_{max} is 84.7 ± 25.0 g C m^{-2} for NF sites and 76.3 ± 25.2 g C m^{-2} for DBF sites (Fig. 3e). On average, a one-day advance in GS_{start} and a one-day delay in GS_{end} increase GPP in spring and autumn by 4.0 ± 2.5 and 4.4 ± 2.6 g C m^{-2}, respectively. A one-day change in GS_{start} and GS_{end} causes the largest GPP changes in spring (6.3 ± 1.8 g C m^{-2}) and autumn (5.6 ± 1.7 g C m^{-2}) for DBF sites. Spring and autumn GPP respond to GS_{start} and GS_{end} in different ways at the NF sites (Fig. 3d and f). A one-day delay in GS_{end} increases GPP by 5.3 ± 3.2 g C m^{-2} in autumn, while a one-day advance in GS_{start} only increases GPP by 2.9 ± 2.5 g C m^{-2} in spring.

The partial correlation analysis between the anomalies of annual GPP and the three indicators shows that annual GPP correlates the
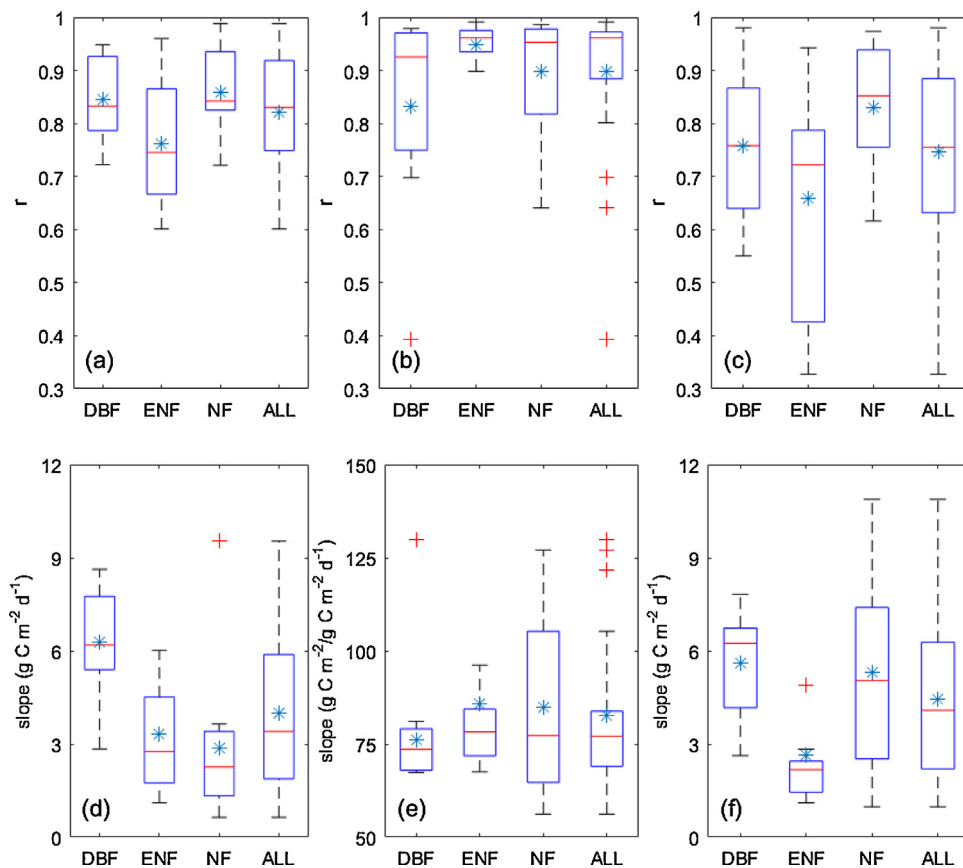
Fig. 3. Distributions of correlation coefficients (r) and regression slopes between the absolute anomalies of (a, d) GS_{start} (day) versus spring GPP (g C m^{-2}), (b, e) GPP_{max} (g C m^{-2} day^{-1}) versus summer GPP, and (c, f) GS_{end} (day) versus autumn GPP for the three PFTs and all of the 27 sites. The mean values of r and regression slopes are shown in asterisks.
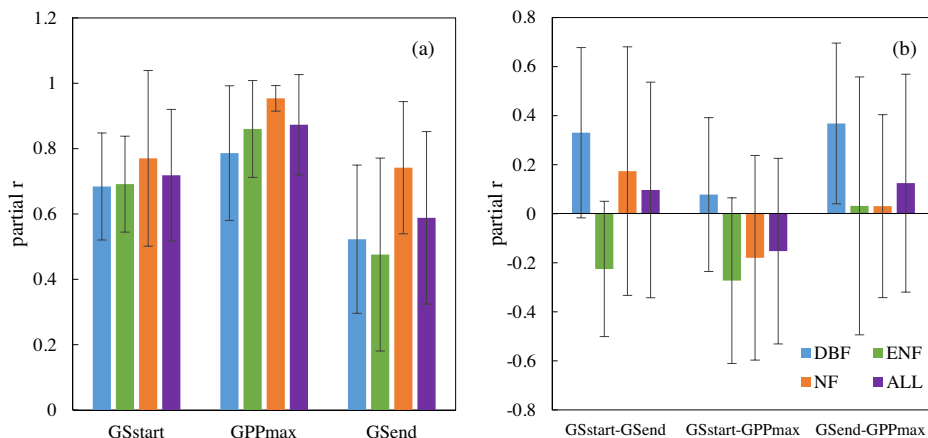

Fig. 4. Partial correlation coefficients (r) (a) between absolute anomalies of annual GPP and the three indicators and (b) between each pair of the three indicators for the three PFTs and all of the 27 sites. The standard deviation of the correlation coefficient is shown in black error bars.

strongest with GPP_{max} (partial r = 0.87 ± 0.15), followed by GS_{start} (partial r = 0.72 ± 0.20) and GS_{end} (partial r = 0.59 ± 0.26) for the 27 sites (Fig. 4a). The partial correlation coefficient with respect to GPP_{max} is more than 0.80 for 23 of the 27 sites, and that with respect to GS_{start} and GS_{end} is more than 0.60 for 19 and 14 sites, respectively. The effects of the two phenological indicators on annual GPP vary over different sites, resulting in large standard deviation of the partial regression coefficients. GPP_{max} for the NF sites correlates the best with annual GPP (r = 0.95 ± 0.04) excluding the effects of the two phenological indicators. Similarly, both GS_{start} and GS_{end} show

stronger partial correlation with annual GPP variation for NF sites than for DBF and ENF sites.

The interrelationships between the three indicators were also investigated for each site. The correlation coefficient is 0.10 ± 0.44 between GS_{start} and GS_{end}, −0.15 ± 0.38 between GS_{start} and GPP_{max}, and 0.12 ± 0.44 between GS_{end} and GPP_{max} (Fig. 4b). Although the interrelationship among the three indicators is strong (with r > 0.7 for any pair of correlation) for several sites (3 DBF, 2 ENF and 2 NF sites), the low mean correlation coefficient and high standard deviation indicate that there is no consistent correlation between each pair of the three indicators across the 27 sites. As the three

indicators individually explain annual GPP variability well, and they are independent from each other to a large extent for most of the 27 sites, the three indicators can be used to establish an integrated statistical model to explain annual GPP variability.

3.2. Statistical model of integrated phenology and physiology for each site

The relative anomalies of the three indicators and annual GPP were calculated and a multiple regression was established to estimate the phenological and physiological sensitivity coefficients in the SMIPP for each of the 27 sites. The coefficient of determination (R^2) of the regression, and the estimated values of the three sensitivity coefficients as well as their significance levels are shown in Table 2. The physiological sensitivity coefficient, m_{gpp}, is significantly different from zero at 0.01 level for 22 sites, and varies from 0.31 to 1.53 and averages at 0.82, indicating that 1 percent change in GPP$_{max}$ would lead to 0.82% change in annual GPP on average (Fig. 5b). Because the two phenological indicators have different effects on annual GPP over different sites, the phenological sensitivity coefficients, m_{start} and m_{end}, show relatively large variability across different sites, ranging from 0.01 to 1.81 and from 0 to 1.39, respectively, and m_{start} is larger than m_{end} for most sites (Fig. 5c and d). Overall, the combination of the three indicators can explain $90 \pm 11\%$ of the variation in annual GPP, and the regression equation is significant at 0.01 level for 21 sites, indicating that the SMIPP can explain the inter-annual GPP variability well.

The NF sites consistently exhibit high R^2 (0.96 ± 0.03) in the SMIPP, suggesting that the three indicators can effectively capture the annual GPP change in non-forest ecosystems. In comparison with NF sites, R^2 varies among the ENF (0.88 ± 0.09) and DBF (0.83 ± 0.15) sites (Fig. 5a). The low value and large variance of R^2 at the DBF sites are largely attributed to two sites, i.e., DE-Hai and IT-Ro2, where GPP$_{max}$ does not capture the summer GPP change, especially during drought years, which will be discussed later. The value of m_{gpp} is much larger for NF sites (0.96 ± 0.24) than that for DBF (0.70 ± 0.18) and ENF (0.76 ± 0.26) sites (Fig. 5b), indicating that annual GPP of NF is more sensitive to GPP$_{max}$. At the NF sites, summer GPP accounts for a larger proportion of annual GPP, thus, 1% change in GPP$_{max}$ would lead to a greater change in annual GPP at the NF sites. The NF sites show high variations in m_{start} and m_{end}, larger than those for the two forest PFTs. In addition, the values of m_{start} and m_{end} are higher for DBF sites, about twice of those for ENF sites (Fig. 5c and d).

3.3. Separating the contributions of the three indicators to annual GPP variability

As the SMIPP shows, the relative anomaly of annual GPP can be separated into three independent components, induced by the changes in the three indicators, respectively. Thus, the products of the relative anomalies of the three indicators by the sensitivity coefficients of annual GPP with respect to them denote the contributions of the three indicators to annual GPP variation. Their contributions vary from site-year to site-year for each PFT (Fig. 6), which are caused by the inter-annual variation of the indicators and the variation of the sensitivity coefficients among different sites. The relative anomalies of the indicators range from −49% to 51% for GS$_{start}$, from −39% to 56% for GPP$_{max}$, and from −70% to 62% for GS$_{end}$ among the 283 site-years. With the sensitivity coefficients for each site in Table 2, the three estimated components of annual GPP relative anomalies vary from −21% to 29% (GS$_{start}$), from −35% to 41% (GPP$_{max}$), and from −21% to 11% (GS$_{end}$), respectively, resulting in a range of −41% to 41% for annual GPP relative anomaly over the 283 site-years (Fig. 6). Combining the three independent components, the estimated annual GPP relative anomalies correlate well with

the observed values both for a certain PFT and all sites. The NF site-years exhibit the highest R^2 (0.98), followed by ENF (0.95) and DBF (0.85) site-years, and the overall R^2 is 0.93 for the 283 site-years. The estimated annual GPP relative anomalies from GPP$_{max}$ are much larger than those from GS$_{start}$ and GS$_{end}$, indicating that GPP$_{max}$ contributes more than GS$_{start}$ and GS$_{end}$ to annual GPP variability for the three PFTs (Fig. 6).

4. Discussion

4.1. Comparison of the SMIPP with other models

In the annual cycle of vegetation growth and dormancy, GPP is controlled by photosynthetic capacity and the growing season length. Our study indicates that the three indicators are closely related to their respective seasonal GPP and the combination of them can explain annual GPP variability to a large extent. The environmental factors, such as temperature, moisture and radiation, affect annual GPP variability through their influences on the three indicators. For example, climate warming accelerates carbon assimilation in spring, which can be captured by earlier GS$_{start}$ in view of the close relationship between warmer temperature and earlier spring emergence in temperate and boreal ecosystems (Keenan et al., 2014; Piao et al., 2015), and the following high temperature in summer may reduce GPP$_{max}$ and summer GPP, because warmer temperature implies higher vapor pressure deficit and exacerbates soil moisture deficits during the middle of the growing season (Angert et al., 2005; Buermann et al., 2013). Because the three indicators can capture the fluctuations in GPP induced by changing environmental conditions, which contribute significantly to the variation in annual GPP (Zscheischler et al., 2014), the proposed SMIPP is able to effectively explain annual GPP variability.

The predictive power of both phenological and physiological indicators, and the combination of them have been explored in previous studies (Richardson et al., 2013; Stoy et al., 2014; Wu et al., 2013; Xia et al., 2015). Here we compared the results of the SMIPP with three single indicator models, i.e., a simplified SMIPP version including only one indicator in Eq. (3), and the statistical model in Xia et al. (2015). The SMIPP is shown to be much more effective than any of the three single indicator models (Fig. 7). The single indicator model which only links to GPP in the corresponding season has limitation in explaining annual GPP variability unless the seasonal GPP correlates strongly with annual GPP. For example, the three seasonal GPP is weakly correlated with annual GPP (spring: r = 0.25; summer: r = 0.69; autumn: r = 0.40) at the US-Ne1 site, and neither of the three single indicator models can explain more than 30% of annual GPP variability. However, the combination of the three indicators in the SMIPP can effectively explain 99.5% of variation in annual GPP. Although a single indicator can capture annual GPP variation in several sites, the SMIPP can consistently explain GPP variability in most sites, indicating that annual GPP variability should be explained simultaneously from plant physiology and spring and autumn phenology.

Xia et al. (2015) reported that $CUP \times GPP_{max}$ well captures the variability in annual GPP, and the ratio α between annual GPP and $CUP \times GPP_{max}$ is relatively constant around 0.62 across abroad range of vegetation types and environmental conditions. In comparison with the statistical model in Xia et al. (2015), the SMIPP explains annual GPP variability by investigating the contributions of the three indicators to the relative change in annual GPP. Although our study does not yield any similar regression coefficients as the stable ratio α in Xia et al. (2015), the results indicate that the SMIPP ($R^2 = 0.90 \pm 0.11$) improves the explanatory power of Xia's model ($R^2 = 0.87 \pm 0.16$) by replacing the phenological indicator CUP with GS$_{start}$ and GS$_{end}$ for the 27 sites (Fig. 7). This study

Table 2

Estimated phenological and physiological sensitivity coefficients, i.e., m_{start}, m_{gpp}, and m_{end}, and the coefficient of determination (R^2) of the SMIPP for each of the 27 sites. The statistically significance (p-value) of the regression equations and sensitivity coefficients are shown as well.

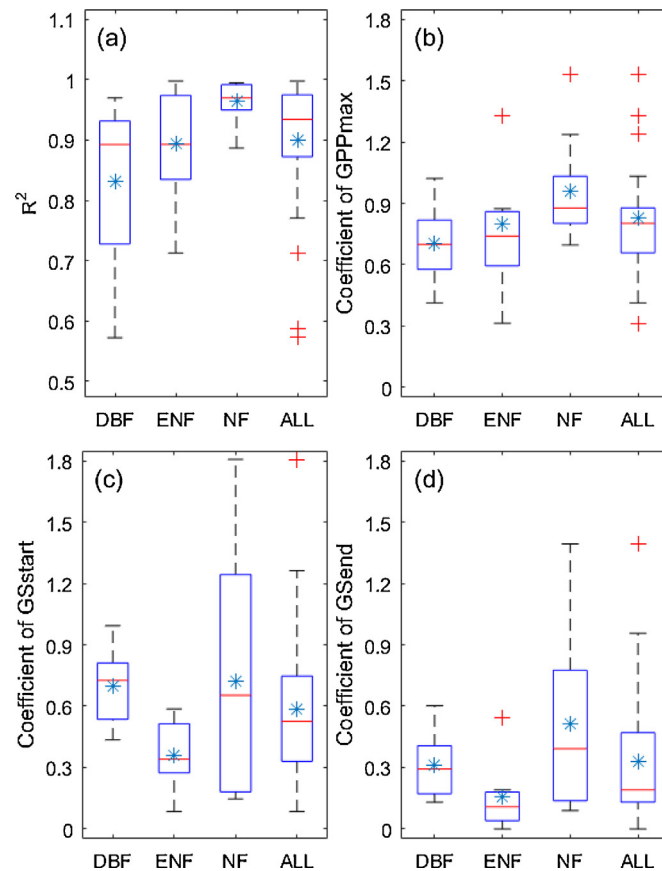| Site ID	PFT	R^2	p-value	m_{start}	p-value	m_{gpp}	p-value	m_{end}	p-value
DE-Hai	DBF	0.57	0.203	0.99	0.185	0.41	0.390	0.17	0.749
ITCol	DBF	0.90	0.001	0.75	0.002	0.52	0.056	0.60	0.031
ITRo2	DBF	0.59	0.087	0.81	0.280	0.75	0.040	0.13	0.470
USHa1	DBF	0.93	<0.001	0.61	<0.001	0.64	<0.001	0.48	0.019
USMMS	DBF	0.87	<0.001	0.43	0.011	1.02	<0.001	0.34	<0.001
USPFa	DBF	0.89	<0.001	0.46	0.017	0.63	<0.001	0.17	0.017
USUMd	DBF	0.93	0.008	0.70	0.064	0.87	0.003	0.26	0.118
USWCr	DBF	0.97	<0.001	0.81	<0.001	0.76	<0.001	0.33	0.175
BEBra	ENF	0.87	0.012	0.08	0.211	0.74	0.009	0.03	0.624
CAQcu	ENF	1.00	<0.001	0.52	0.003	0.84	<0.001	0.11	0.347
CAQfo	ENF	0.90	0.054	0.59	0.058	1.33	0.049	0.54	0.079
CHDav	ENF	0.71	0.008	0.21	0.154	0.31	0.127	0.11	0.096
FISod	ENF	0.97	<0.001	0.51	0.028	0.61	0.001	0.00	0.996
ITRen	ENF	0.98	<0.001	0.29	0.011	0.87	<0.001	0.19	0.001
RUFyo	ENF	0.86	<0.001	0.42	0.039	0.86	<0.001	0.18	0.093
USHo1	ENF	0.89	<0.001	0.32	0.022	0.74	0.001	0.13	0.013
USHo2	ENF	0.77	0.006	0.34	0.048	0.56	0.003	0.04	0.600
USNe1	CRO	1.00	<0.001	1.26	<0.001	0.88	<0.001	0.78	<0.001
USNe2	CRO	0.99	<0.001	0.71	0.028	1.03	<0.001	0.56	0.007
USNe3	CRO	0.99	<0.001	1.81	0.001	0.88	<0.001	1.39	0.005
ATNeu	GRA	0.94	0.002	0.15	0.011	1.53	0.003	0.14	0.027
ITMBo	GRA	0.89	0.001	0.60	0.005	1.24	0.002	0.33	0.020
SEDeg	GRA	0.95	0.001	0.17	0.759	0.73	0.005	0.30	0.425
UKAMo	GRA	0.95	0.068	0.38	0.011	0.80	0.002	0.13	0.155
USKon	GRA	0.96	0.012	0.18	0.395	0.87	0.010	0.09	0.439
USLos	CSH	0.98	<0.001	0.75	0.001	0.70	<0.001	0.45	0.002
FIKaa	WET	0.99	<0.001	1.24	<0.001	0.92	<0.001	0.96	0.002

Fig. 5. Distributions of (a) R^2, and the sensitivity coefficients of (b) GPP_{max}, (c) GS_{start}, and (d) GS_{end} in the SMIPP for the three PFTs and all of the 27 sites. The mean values of the sensitivity coefficients are shown in asterisks.

shows that the three sensitivity coefficients vary among different sites, and the sensitivity coefficients with respect to GS_{start} and GS_{end} are not consistent for individual sites. The different sensi-

tivity coefficients of annual GPP to GS_{start} and GS_{end} at the 27 sites indicate that the responses of annual GPP to GS_{start} and GS_{end} are not identical (Fig. 5c and d). Thus, although CUP integrates spring and
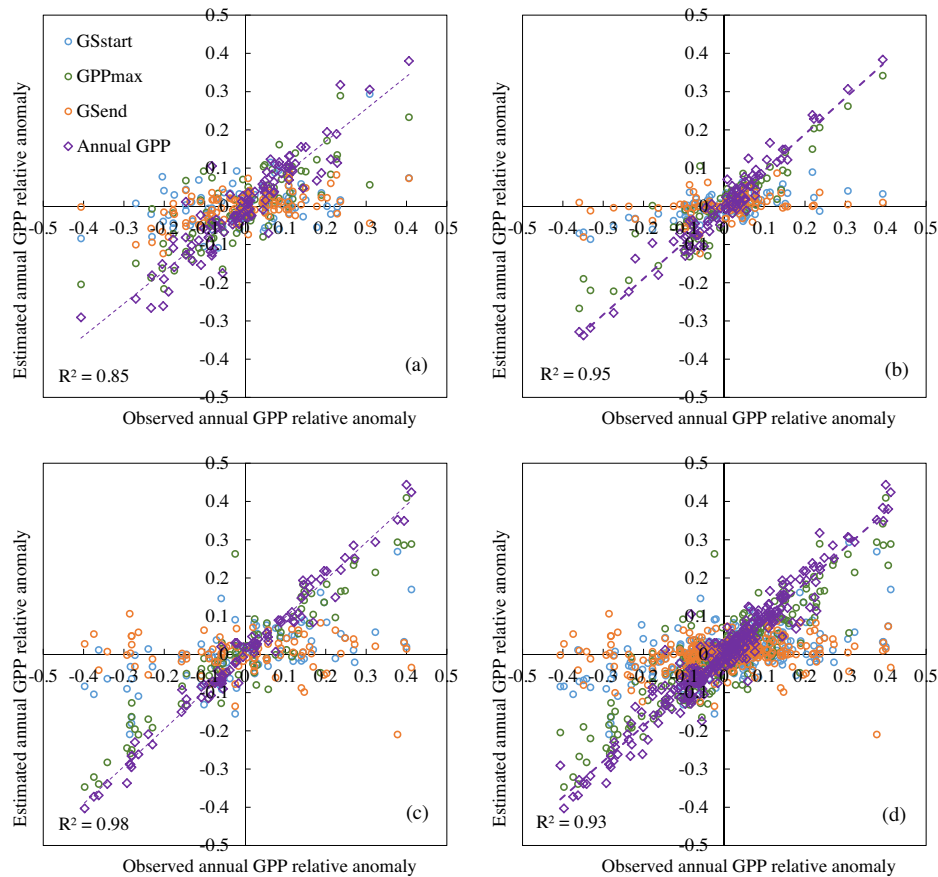
Fig. 6. Linear relationship between the observed and estimated annual GPP relative anomaly for (a) DBF; (b) ENF; (c) NF; and (d) all the 283 site-years based on the SMIPP for each site. The three components of the estimated relative anomaly induced by the three indicators are also shown.

autumn phenology together, it cannot fully reflect the phenological effects on annual GPP. The non-identical responses of annual GPP to GS_{start} and GS_{end} may be attributed to the different environmental conditions in spring and autumn, and the different triggering mechanisms of spring emergence and autumn senescence (Menzel et al., 2006; Vitasse et al., 2009). Through distinguishing the effects of both GS_{start} and GS_{end} on annual GPP, the SMIPP can better reflect the effects of plant phenological and physiological changes on annual GPP change, and separate the respective contributions of GS_{start}, GPP_{max}, and GS_{end} to annual GPP change based on the sensitivity coefficients of annual GPP to them.

4.2. Annual GPP variability among ecosystem types

The SMIPP indicates that annual GPP variability is attributed to the phenological and physiological changes induced by environmental factors. The different responses of the three indicators to environmental changes and the combined explanatory power of the three indicators to annual GPP variability are associated with ecosystem types. Correlation analyses indicate that GPP_{max} explains summer GPP the best for ENF sites, with both the highest correlation coefficient and regression slope among the three PFTs. However, GS_{start} and GS_{end} explain spring and autumn GPP the least for ENF sites. At ENF sites, where the seasonality of vegetation canopy is low, seasonal GPP variations are mainly caused by physiological changes. Both physiological and canopy (leaf-on and leaf off) changes contribute substantially to GPP variations at DBF and NF sites (Flanagan et al., 2002; Gamon et al., 1995; Ito et al., 2006; Royer et al., 2005; Saigusa et al., 2002). Smaller sensitivity coefficients with respect to GS_{start} and GS_{end} are also found for ENF

sites than the other two PFTs in the SMIPP. The results reported by Richardson et al. (2010) also indicate that the productivity of ENF is less sensitive to phenological changes than that of DBF.

In comparison with forest ecosystems, the three indicators explain annual GPP variation better for non-forest ecosystems. The partial correlation analyses present stronger relationship between each of the three indicators and annual GPP for NF than for DBF and ENF sites. In general, the distinct seasonal changes make it easier to track the changes in plant phenology and physiology, and hence annual GPP change at the NF sites. In comparison with forest ecosystems, which are more adaptive to environmental changes and can resist the environmental stresses below a certain threshold, non-forest ecosystems generally have poor self-regulation abilities under environmental stresses (Kozlowski & Pallardy, 2002; Niinemets, 2010; Teuling et al., 2010). Thus, non-forests respond more quickly and intensively to environmental changes, while forests always respond to environmental changes with a delay (Zhang et al., 2016). Consequently, the impact of environmental changes on annual GPP can be better captured by the three indicators, and the SMIPP involving the three indicators can explain the inter-annual GPP variability more effectively for NF sites. The delayed and complicated responses of forests to environmental changes make it hard to track GPP variations with the three indicators at several sites, especially during drought periods.

4.3. Explanatory power of the SMIPP during drought years

Terrestrial ecosystems are closely coupled with the climate system. The carbon cycle is susceptible to climate change, and it also affects global climate through ecosystem feedback loops (Heimann
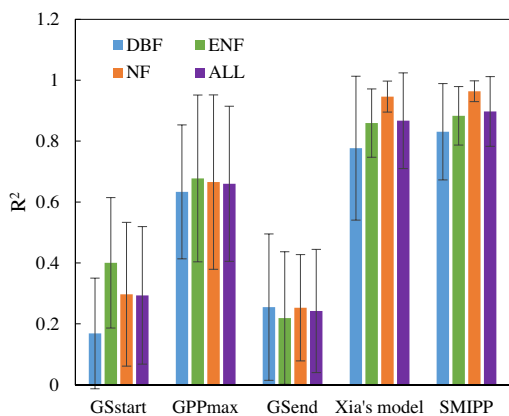
Fig. 7. Coefficient of determination (R^2) between the estimated and observed annual GPP relative anomalies using the three single indicator models, i.e., GS_{start}, GPP_{max}, and GS_{end}, the statistical model in Xia et al. (2015), and the SMIPP for the three PFTs and all of the 27 sites. The standard deviation of the correlation coefficient is shown in black error bars.

and Reichstein, 2008; Luo, 2007). More and more extreme climate events have happened in recent years and significantly influenced the carbon cycle (Reichstein et al., 2013). Drought is one of the climate extremes which greatly reduce terrestrial carbon uptake (Allen et al., 2009; Zeng et al., 2005; Zhao and Running, 2010), and it brings a big challenge for the SMIPP to capture the responses to drought among different ecosystems.

Taking the 2003 European drought as an example, the four sites, i.e., IT-Ren (ENF), IT-MBo (NF), IT-Ro2 (DBF), and DE-Hai (DBF), experienced extreme drought from June through October (Ciais et al., 2005). At the IT-Ren site, the forests tolerated water deficits and maintained their canopy structure during the initial phase of drought stress, and spring and summer GPP only decreased by 1.1% and 4.6%, respectively. GPP_{max}, which decreased by 5.9%, tracked the GPP decline in summer. The combination of the three indicators well explained ($R^2 = 0.93$) the annual GPP reduction of 9.7%. Warmer spring triggered more leaves and enhanced carbon uptake for NF and DBF under slight drought stress at the IT-MBo, IT-Ro2 and DE-Hai sites. Soon after they suffered severe water stress, which led to GPP decline in summer, by 14.3%, 23.4% and 11.6%, respectively. GPP_{max} emerged at early June at the three sites, more than 10 days earlier than their mean dates, and it declined only by 4.4% at the IT-MBo and even grew by 9.9% and 4.0% at the IT-Ro2 and DE-Hai sites. Obviously, GPP_{max} did not fully reveal the drought effect on plant physiology, which reduced the explanatory power of the SMIPP.

It is worth noting that the IT-Ro2 is located in Mediterranean-climate region where drought occurs frequently in summer. During drought years, GPP dropped down in late summer and then recovered slightly in early autumn, and GPP_{max} appeared much earlier than normal years. In most sites, GPP_{max} could successfully perceive the physiological changes and reflect summer GPP variations, and the time lag between GPP_{max} and drought induced GPP decline can reduce the explanatory power of the SMIPP. It is also reported that the joint control of CUP and GPP_{max} on annual GPP variability is weak in tropical and Mediterranean climates (Xia et al., 2015). On the one hand, the relationship between GPP_{max} and summer GPP is weak due to frequent summer drought; on the other hand, it is hard to determine GS_{start} and GS_{end} which can effectively reflect phenological changes in tropical and Mediterranean climates. Thus, more specified investigation into plant responses to drought is needed in order to successfully perceive the phenological and physiological changes in plants and better explain annual GPP variability in tropical and Mediterranean climates.

4.4. Limitations and implications of the SMIPP under changing climate

The SMIPP works well for the ecosystems with distinct seasonal patterns, however, its explanatory power is limited in Mediterranean and tropical ecosystems. In addition, the assumption of the three independent indicators is needed in the SMIPP in order to separate the contributions of them to annual GPP variability. Although the correlation analysis in this study shows that the three indicators are independent from each other for most sites, several earlier studies indicate that they might be interrelated as the terrestrial ecosystems respond to climate change through both phenological and physiological changes. Buermann et al. (2013) suggested that warming induced earlier springs may decrease summer GPP_{max} in North American boreal forests. And it was found that the timing of autumn senescence is also influenced by spring phenology in temperate deciduous forests across eastern US (Keenan and Richardson, 2015). Those phenomena are yet to be quantitatively evaluated to assess the degree of the interrelationships between the three indicators.

This study was based on the Fluxnet data at the ecosystem scale, and the SMIPP can be extended to explain and predict annual GPP variability at a regional or global scale with remote sensing data. The phenological and physiological changes can be inferred from remote sensing or webcam products to estimate annual GPP dynamics. In many studies, the phenological transitions are determined using satellite-derived vegetation indices, such as normalized difference vegetation index (NDVI) and enhanced vegetation index (EVI) (Cao et al., 2015; Garrity et al., 2011; Gonsamo et al., 2012). The remotely derived sun-induced chlorophyll fluorescence (SIF) data are closely related to vegetation photosynthetic physiology (Damm et al., 2010; Joiner et al., 2014; Rossini et al., 2015), and the relationship between SIF and maximum daily GPP can be further established. Thus, the three indicators derived from remote sensing products may be used to interpret the inter-annual variability of GPP at the global scale.

5. Conclusions

This study shows that annual GPP anomaly is strongly correlated with the anomaly of GS_{start}, GPP_{max}, and GS_{end} using data from 27 flux tower sites across North America and Europe. Combining the three indicators, the SMIPP can explain $90 \pm 11\%$ of the annual GPP variability among the 27 sites, and it is more effective than both the single indicator models and the statistical model in Xia et al. (2015). For each site-year, the contributions of GS_{start}, GPP_{max}, and GS_{end} to annual GPP variation can be separated using the relative anomalies of the three indicators and the sensitivity coefficients in the SMIPP. In general, GPP_{max} contributes more than GS_{start} and GS_{end} to annual GPP variation at the 27 sites. This study indicates that the influence of climatic and environmental changes on annual GPP can be evaluated based on the three indicators within the SMIPP framework, and also elucidates that annual GPP variation can be estimated by investigating the phenological and physiological changes in terrestrial ecosystems under future climate change.

References

Allard, V., Ourcival, J.M., Rambal, S., Joffre, R., Rocheteau, A., 2008. Seasonal and annual variation of carbon exchange in an evergreen Mediterranean forest in southern France. Glob. Change Biol. 14, 714–725.

Allen, C.D., Macalady, A.K., Chenchouni, H., et al., 2009. A global overview of drought and heat induced tree mortality reveals emerging climate change risk for forests. For. Ecol. Manag. 259, 660–684.

Angert, A., Biraud, S., Bonfils, C., et al., 2005. Drier summers cancel out the CO$_2$ uptake enhancement induced by warmer springs. Proc. Nat. Acad. Sci. U. S. A. 102, 10823–10827.

Aurela, M., Laurila, T., Tuovinen, J.P., 2004. The timing of snow melt controls the annual CO$_2$ balance in a subarctic fen. Geophys. Res. Lett. 31, 3–6.

Austin, P.C., Steyerberg, E.W., 2015. The number of subjects per variable required in linear regression analyses. J. Clin. Epidemiol. 68 (6), 627–636.

Ballantyne, A.P., Alden, C.B., Miller, J.B., Tans, P.P., White, J.W.C., 2012. Increase in observed net carbon dioxide uptake by land and oceans during the past 50 years. Nature 488, 70–72.

Bergeron, O., Margolis, H.A., Black, T.A., Coursolle, C., Dunn, A.L., Barr, A.G., Wofsy, S.C., 2007. Comparison of carbon dioxide fluxes over three boreal black spruce forests in Canada. Glob. Change Biol. 13, 89–107.

Buermann, W., Bikash, P.R., Jung, M., Burn, D.H., Reichstein, M., 2013. Earlier springs decrease peak summer productivity in North American boreal forests. Environ. Res. Lett. 8, 024027.

Cao, R., Chen, J., Shen, M., Tang, Y., 2015. An improved logistic method for detecting spring vegetation phenology in grasslands from MODIS EVI time-series data. Agric. For. Meteorol. 200, 9–20.

Carrara, A., Janssens, I.A., Curiel Yuste, J., Ceulemans, R., 2004. Seasonal changes in photosynthesis, respiration and NEE of a mixed temperate forest. Agric. For. Meteorol. 126, 15–31.

Chen, H., Zhu, Q., Wu, N., Wang, Y., Peng, C.H., 2011. Delayed spring phenology on the Tibetan Plateau may also be attributable to other factors than winter and spring warming. Proc. Natl. Acad. Sci. U. S. A. 108, E93.

Churkina, G., Schimel, D., Braswell, B.H., Xiao, X.M., 2005. Spatial analysis of growing season length control over net ecosystem exchange. Glob. Change Biol. 11, 1777–1787.

Ciais, P., Reichstein, M., Viovy, N., et al., 2005. Europe-wide reduction in primary productivity caused by the heat and drought in 2003. Nature 437, 529–533.

Cleland, E.E., Chuine, I., Menzel, A., Mooney, H.A., Schwartz, M.D., 2007. Shifting plant phenology in response to global change. Trends Ecol. Evol. 22, 357–365.

Damm, A., Elber, J., Erler, A., et al., 2010. Remote sensing of sun-induced fluorescence to improve modeling of diurnal courses of gross primary production (GPP). Glob. Change Biol. 16, 171–186.

Dragoni, D., Schmid, H.P., Grimmond, C.S.B., Loescher, H.W., 2007. Uncertainty of annual net ecosystem productivity estimated using eddy covariance flux measurements. J. Geophys. Res. 112, 1–9.

Dragoni, D., Schmid, H.P., Wayson, C.A., Potter, H., Grimmond, C.S.B., Randolph, J.C., 2011. Evidence of increased net ecosystem productivity associated with a longer vegetated season in a deciduous forest in south-central Indiana, USA. Glob. Change Biol. 17, 886–897.

Flanagan, L.B., Wever, L.A., Carlson, P.J., 2002. Seasonal and interannual variation in carbon dioxide exchange and carbon balance in a northern temperate grassland. Glob. Change Biol. 8, 599–615.

Fracheboud, Y., Luquez, V., Björkén, L., Sjödin, A., Tuominen, H., Jansson, S., 2009. The control of autumn senescence in European aspen. Plant Physiol. 149, 1982–1991.

Fu, Y.H., Zhao, H., Piao, S., et al., 2015. Declining global warming effects on the phenology of spring leaf unfolding. Nature 526, 104–107.

Gamon, J.A., Gamon, J.A., Field, C.B., et al., 1995. Relationships between NDVI, canopy structure, and photosynthesis in three California vegetation types. Ecol. Appl. 5, 28–41.

Garonna, I., De Jong, R., De Wit, A.J.W., Mücher, C.A., Schmid, B., Schaepman, M.E., 2014. Strong contribution of autumn phenology to changes in satellite-derived growing season length estimates across Europe (1982–2011). Glob. Change Biol. 20, 3457–3470.

Garrity, S.R., Bohrer, G., Maurer, K.D., Mueller, K.L., Vogel, C.S., Curtis, P.S., 2011. A comparison of multiple phenology data sources for estimating seasonal transitions in deciduous forest carbon exchange. Agric. For. Meteorol. 151, 1741–1752.

Giasson, M.A., Coursolle, C., Margolis, H.A., 2006. Ecosystem-level CO$_2$ fluxes from a boreal cutover in eastern Canada before and after scarification. Agric. For. Meteorol. 140, 23–40.

Gilmanov, T.G., Soussana, J.F., Aires, L., et al., 2007. Partitioning European grassland net ecosystem CO$_2$ exchange into gross primary productivity and ecosystem respiration using light response function analysis. Agr. Ecosyst. Environ. 121, 93–120.

Gioli, B., Miglietta, F., De Martino, B., et al., 2004. Comparison between tower and aircraft-based eddy covariance fluxes in five European regions. Agric. For. Meteorol. 127, 1–16.

Gonsamo, A., Chen, J.M., David, T.P., Kurz, W.A., Wu, C., 2012. Land surface phenology from optical satellite measurement and CO$_2$ eddy covariance technique. J. Geophys. Res. G: Biogeosci. 117, 1–18.

Groenendijk, M., van der Molen, M.K., Dolman, A.J., 2009. Seasonal variation in ecosystem parameters derived from FLUXNET data. Biogeosci. Discuss. 6, 2863–2912.

Heimann, M., Reichstein, M., 2008. Terrestrial ecosystem carbon dynamics and climate feedbacks. Nature 451, 289–292.

Hirata, R., Hirano, T., Saigusa, N., et al., 2007. Seasonal and interannual variations in carbon dioxide exchange of a temperate larch forest. Agric. For. Meteorol. 147, 110–124.

Hollinger, D.Y., Aber, J., Dail, B., et al., 2004. Spatial and temporal variability in forest-atmosphere CO$_2$ exchange. Global Change Biol. 10, 1689–1706.

Ibáñez, I., Primack, R.B., Miller-Rushing, A.J., et al., 2010. Forecasting phenology under global warming. Philos. Trans. R. Soc. B 365, 3247–3260.

Ito, A., Muraoka, H., Koizumi, H., Saigusa, N., Murayama, S., Yamamoto, S., 2006. Seasonal variation in leaf properties and ecosystem carbon budget in a cool-temperate deciduous broad-leaved forest: simulation analysis at Takayama site. Jpn. Ecol. Res. 21, 137–149.

Jeong, S.J., Ho, C.H., Gim, H.J., Brown, M.E., 2011. Phenology shifts at start vs. end of growing season in temperate vegetation over the Northern Hemisphere for the period 1982–2008. Glob. Change Biol. 17, 2385–2399.

Joiner, J., Yoshida, Y., Vasilkov, A., et al., 2014. The seasonal cycle of satellite chlorophyll fluorescence observations and its relationship to vegetation phenology and ecosystem atmosphere carbon exchange. Remote Sens. Environ. 152, 375–391.

Keenan, T.F., Richardson, A.D., 2015. The timing of autumn senescence is affected by the time of spring phenology: implications for predictive models. Glob. Change Biol. 21, 2634–2641.

Keenan, T.F., Gray, J., Friedl, M.A., et al., 2014. Net carbon uptake has increased through warming-induced changes in temperate forest phenology. Nat. Clim. Change 4, 598–604.

Kozlowski, T.T., Pallardy, S.G., 2002. Acclimation and adaptive responses of woody plants to environmental stresses. Bot. Rev. 68, 270–334.

Kutsch, W.L., Kolle, O., Rebmann, C., Knohl, A., Ziegler, W., Schulze, E.D., 2008. Advection and resulting CO$_2$ exchange uncertainty in a tall forest in central Germany. Ecol. Appl. 18, 1391–1405.

Liang, S., Zheng, T., Liu, R., Fang, H., Tsay, S.C., Running, S., 2006. Estimation of incident photosynthetically active radiation from Moderate Resolution Imaging Spectrometer data. J. Geophys. Res. 111, 1–13.

Lund, M., Lafleur, P.M., Roulet, N.T., et al., 2010. Variability in exchange of CO$_2$ across 12 northern peatland and tundra sites. Global Change Biol. 16, 2436–2448.

Luo, Y., Keenan, T.F., Smith, M., 2015. Predictability of the terrestrial carbon cycle. Glob. Change Biol. 21, 1737–1751.

Luo, Y., 2007. Terrestrial Carbon—Cycle feedback to climate warming. Annu. Rev. Ecol. Evol. Syst. 38, 683–712.

Menzel, A., Fabian, P., 1999. Growing season extended in Europe. Nature 397, 659.

Menzel, A., Sparks, T.H., Estrella, N., et al., 2006. European phenological response to climate change matches the warming pattern. Glob. Change Biol. 12, 1969–1976.

Nave, L.E., Gough, C.M., Maurer, K.D., et al., 2011. Disturbance and the resilience of coupled carbon and nitrogen cycling in a north temperate forest. J. Geophys. Res. G: Biogeosci. 116, 1–14.

Niinemets, Ü., 2010. Responses of forest trees to single and multiple environmental stresses from seedlings to mature plants: past stress history, stress interactions, tolerance and acclimation. For. Ecol. Manag. 260, 1623–1639.

Panchen, Z.A., Primack, R.B., Gallinat, A.S., Nordt, B., Stevens, A., Du, Y., Fahey, R., 2015. Substantial variation in leaf senescence times among 1360 temperate woody plant species: implications for phenology and ecosystem processes. Ann. Bot. 116, 865–873.

Papale, D., Valentini, R., 2003. A new assessment of European forests carbon exchanges by eddy fluxes and artificial neural network spatialization. Glob. Change Biol. 9, 525–535.

Piao, S., Friedlingstein, P., Ciais, P., Viovy, N., Demarty, J., 2007. Growing season extension and its impact on terrestrial carbon cycle in the Northern Hemisphere over the past 2 decades. Glob. Biogeochem. Cycl. 21, GB3018.

Piao, S., et al., 2015. Leaf onset in the northern hemisphere triggered by daytime temperature. Nat. Commun. 6, 6911.

Pope, K.S., Dose, V., Da Silva, D., Brown, P.H., Leslie, C.A., Dejong, T.M., 2013. Detecting nonlinear response of spring phenology to climate change by Bayesian analysis. Glob. Change Biol. 19, 1518–1525.

Reichstein, M., Falge, E., Baldocchi, D., et al., 2005. On the separation of net ecosystem exchange into assimilation and ecosystem respiration: review and improved algorithm. Glob. Change Biol. 11, 1424–1439.

Reichstein, M., Bahn, M., Ciais, P., et al., 2013. Climate extremes and the carbon cycle. Nature 500, 287–295.

Richardson, A.D., Hollinger, D.Y., 2005. Statistical modeling of ecosystem respiration using eddy covariance data: maximum likelihood parameter

estimation, and Monte Carlo simulation of model and parameter uncertainty, applied to three simple models. Agric. For. Meteorol. 131, 191–208.

Richardson, A.D., Black, T.A., Ciais, P., et al., 2010. Influence of spring and autumn phenological transitions on forest ecosystem productivity. Philos. Trans. R. Soc. B 365, 3227–3246.

Richardson, A.D., Keenan, T.F., Migliavacca, M., Ryu, Y., Sonnentag, O., Toomey, M., 2013. Climate change, phenology, and phenological control of vegetation feedbacks to the climate system. Agric. For. Meteorol. 169, 156–173.

Rossini, M., Nedbal, L., Guanter, L., et al., 2015. Red and far red Sun-induced chlorophyll fluorescence as a measure of plant photosynthesis. Geophys. Res. Lett. 42, 1632–1639.

Royer, D.L., Osborne, C.P., Beerling, D.J., 2005. Contrasting seasonal patterns of carbon gain in evergreen and deciduous trees of ancient polar forests. Paleobiology 31, 141–150.

Saigusa, N., Yamamoto, S., Murayama, S., Kondo, H., Nishimura, N., 2002. Gross primary production and net ecosystem exchange of a cool-temperate deciduous forest estimated by the eddy covariance method. Agric. For. Meteorol. 112, 203–215.

Saigusa, N., Yamamoto, S., Hirata, R., et al., 2008. Temporal and spatial variations in the seasonal patterns of CO_2 flux in boreal, temperate, and tropical forests in East Asia. Agric. For. Meteorol. 148, 700–713.

Saito, M., Maksyutov, S., Hirata, R., Richardson, A.D., 2009. An empirical model simulating long-term diurnal CO_2 flux for diverse vegetation types. Biogeosciences 6, 585–599.

Schwalm, C.R., Williams, C.A., Schaefer, K., et al., 2012. Reduction in carbon uptake during turn of the century drought in western North America. Nat. Geosci. 5, 551–556.

Scurlock, J.M.O., Johnson, K., Olson, R.J., 2002. Estimating net primary productivity from grassland biomass dynamics measurements. Glob. Change Biol. 8, 736–753.

Stoy, P.C., Mauder, M., Foken, T., et al., 2013. A data-driven analysis of energy balance closure across FLUXNET research sites: the role of landscape scale heterogeneity. Agric. For. Meteorol. 171–172, 137–152.

Stoy, P.C., Trowbridge, A.M., Bauerle, W.L., 2014. Controls on seasonal patterns of maximum ecosystem carbon uptake and canopy-scale photosynthetic light response: contributions from both temperature and photoperiod. Photosynth. Res. 119, 49–64.

Suyker, A.E., Verma, S.B., Burba, G.G., Arkebauer, T.J., 2005. Gross primary production and ecosystem respiration of irrigated maize and irrigated soybean during a growing season. Agric. For. Meteorol. 131, 180–190.

Teuling, A.J., Seneviratne, S.I., Stöckli, R., et al., 2010. Contrasting response of European forest and grassland energy exchange to heatwaves. Nat. Geosci. 3, 722–727.

Thum, T., Aalto, T., Laurila, T., Aurela, M., Kolari, P., Hari, P., 2007. Parametrization of two photosynthesis models at the canopy scale in a northern boreal Scots pine forest. Tellus B 59, 874–890.

Uehlinger, U., 2006. Annual cycle and inter-annual variability of gross primary production and ecosystem respiration in a floodprone river during a 15-year period. Freshwater Biol. 51, 938–950.

Urbanski, S., Barford, C., Wofsy, S., et al., 2007. Factors controlling CO_2 exchange on timescales from hourly to decadal at Harvard Forest. J. Geophys. Res. G: Biogeosci. 112, 1–25.

Valentini, R., DeAngelis, P., Matteucci, G., Monaco, R., Dore, S., Mugnozza, G.E.S., 1996. Seasonal net carbon dioxide exchange of a beech forest with the atmosphere. Glob. Change Biol. 2, 199–207.

Vautard, R., Yiou, P., Ghil, M., 1992. Singular-spectrum analysis: a toolkit for short, noisy chaotic signals. Physics D 58, 95–126.

Vitasse, Y., Porté, A.J., Kremer, A., Michalet, R., Delzon, S., 2009. Responses of canopy duration to temperature changes in four temperate tree species: relative contributions of spring and autumn leaf phenology. Oecologia 161, 187–198.

Wohlfahrt, G., Anderson-Dunn, M., Bahn, M., et al., 2008. Biotic, abiotic, and management controls on the net ecosystem CO_2 exchange of European mountain grassland ecosystems. Ecosystems 11, 1338–1351.

Wu, C., Chen, J.M., Black, T.A., et al., 2013. Interannual variability of net ecosystem productivity in forests is explained by carbon flux phenology in autumn. Glob. Ecol. Biogeogr. 22, 994–1006.

Xia, J., Niu, S., Ciais, P., et al., 2015. Joint control of terrestrial gross primary productivity by plant phenology and physiology. Proc. Natl. Acad. Sci. U. S. A. 112, 2788–2793.

Yang, Y., Guan, H., Shen, M., Liang, W., Jiang, L., 2015. Changes in autumn vegetation dormancy onset date and the climate controls across temperate ecosystems in China from 1982 to 2010. Glob. Change Biol. 21, 652–665.

Yi, S., Zhou, Z., 2011 Increasing contamination might have delayed spring phenology on the Tibetan Plateau. Proc. Nat. Acad. Sci. U. S. A., 108, E94; author reply E95.

Yi, C., Davis, K.J., Bakwin, P.S., et al., 2004. Observed covariance between ecosystem carbon exchange and atmospheric boundary layer dynamics at a site in northern Wisconsin. J. Geophys. Res. D: Atmos. 109, 1–9.

Yu, H., Luedeling, E., Xu, J., 2010. Winter and spring warming result in delayed spring phenology on the Tibetan Plateau. Proc. Natl. Acad. Sci. U. S. A. 107, 22151–22156.

Zeng, N., Qian, H., Roedenbeck, C., Heimann, M., 2005. Impact of 1998–2002 midlatitude drought and warming on terrestrial ecosystem and the global carbon cycle. Geophys. Res. Lett. 32, 1–4.

Zhang, Y., Xiao, X., Zhou, S., Ciais, P., McCarthy, H., Luo, Y., 2016. Canopy and physiological limitation of GPP during drought and heat wave. Geophys. Res. Lett. 43, 3325–3333.

Zhao, M., Running, S.W., 2010. Drought-Induced Reduction in Global terrestrial net primary production from 2000 through 2009. Science 329, 940–943.

Zhu, W., Tian, H., Xu, X., Pan, Y., Chen, G., Lin, W., 2012. Extension of the growing season due to delayed autumn over mid and high latitudes in North America during 1982–2006. Glob. Ecol. Biogeogr. 21, 260–271.

Zscheischler, J., et al., 2014. A few extreme events dominate global interannual variability in gross primary production. Environ. Res. Lett. 9, 035001.

van Gorsel, E., Delpierre, N., Leuning, R., et al., 2009. Estimating nocturnal ecosystem respiration from the vertical turbulent flux and change in storage of CO_2. Agric. For. Meteorol. 149, 1919–1930.

Zweifel, R., Eugster, W., Etzold, S., Dobbertin, M., Buchmann, N., Häsler, R., 2010. Link between continuous stem radius changes and net ecosystem productivity of a subalpine Norway spruce forest in the Swiss Alps. New Phytol. 187, 819–830.